# Flexible chiral metamaterials in the terahertz regime: a comparative study of various designs

**G. Kenanakis,[1,2,*] R. Zhao,[3] A. Stavrinidis,[1] G. Konstantinidis,[1] N. Katsarakis,[1,2] M. Kafesaki,[1,4] C. M. Soukoulis,[1,5] and E. N. Economou[1]**

[1]*Institute of Electronic Structure and Laser, Foundation for Research & Technology-Hellas, P.O. Box 1385, Vassilika Vouton, 711 10 Heraklion, Crete, Greece*

[2]*Science Department, School of Applied Technology, Technological Educational Institute of Crete, 710 04 Heraklion, Crete, Greece*

[3]*The Blackett Laboratory, Department of Physics, Imperial College London, London SW7 2AZ, United Kingdom*

[4]*Materials Science and Technology Department, University of Crete, 710 03 Heraklion, Crete, Greece*

[5]*Ames Laboratory-USDOE, and Department of Physics and Astronomy, Iowa State University, Ames, Iowa 50011, USA*

**gkenanak@iesl.forth.gr*

**Abstract:** Five different chiral metamaterials in the terahertz (THz) regime, fabricated on fully flexible polyimide substrates, are comparatively studied via numerical calculations and experimental measurements. The chiral properties of these metamaterials, which are discussed based on their optical activity, circular dichroism, and the retrieved effective parameters, show pronounced pure optical activity (larger than 300°/wavelength), as well as important circular polarization generation and filtering capabilities. Negative refractive index is also obtained for all the considered designs.



**OCIS codes:** (160.3918) Metamaterials; (160.1585) Chiral media.

## References and links

1. V. G. Veselago, "The electrodynamics of substances with simultaneously negative values of ε and μ," Sov. Phys. Usp. **10**(4), 509–514 (1968).
2. D. R. Smith, J. B. Pendry, and M. C. Wiltshire, "Metamaterials and negative refractive index," Science **305**(5685), 788–792 (2004).
3. C. M. Soukoulis, M. Kafesaki, and E. N. Economou, "Negative index materials: new frontiers in optics," Adv. Mater. **18**(15), 1941–1952 (2006).
4. V. M. Shalaev, "Optical negative-index metamaterials," Nat. Photonics **1**(1), 41–48 (2007).
5. C. M. Soukoulis, S. Linden, and M. Wegener, "Physics. Negative refractive index at optical wavelengths," Science **315**(5808), 47–49 (2007).
6. M. Wegener and S. Linden, "Giving light yet another new twist," Physics **2**, 3–6 (2009).
7. J. Zhou, D. R. Chowdhury, R. Zhao, A. K. Azad, H. Chen, C. M. Soukoulis, A. J. Taylor, and J. F. O'Hara, "Terahertz chiral metamaterials with giant and dynamically tunable optical activity," Phys. Rev. B **86**(3), 035448 (2012).
8. J. K. Gansel, M. Thiel, M. S. Rill, M. Decker, K. Bade, V. Saile, G. von Freymann, S. Linden, and M. Wegener, "Gold helix photonic metamaterial as broadband circular polarizer," Science **325**(5947), 1513–1515 (2009).
9. R. Zhao, J. Zhou, Th. Koschny, E. N. Economou, and C. M. Soukoulis, "Repulsive Casimir force in chiral metamaterials," Phys. Rev. Lett. **103**(10), 103602 (2009).
10. R. Zhao, Th. Koschny, E. N. Economou, and C. M. Soukoulis, "Repulsive Casimir forces with finite-thickness slabs," Phys. Rev. B **83**(7), 075108 (2011).
11. J. B. Pendry, "A chiral route to negative refraction," Science **306**(5700), 1353–1355 (2004).
12. S. Tretyakov, A. Sihvola, and L. Jylhä, "Backward-wave regime and negative refraction in chiral composites," Photonics Nanostruct. Fundam. Appl. **3**(2-3), 107–115 (2005).
13. V. A. Fedotov, P. L. Mladyonov, S. L. Prosvirnin, A. V. Rogacheva, Y. Chen, and N. I. Zheludev, "Asymmetric propagation of electromagnetic waves through a planar chiral structure," Phys. Rev. Lett. **97**(16), 167401 (2006).
14. E. Plum, V. A. Fedotov, and N. I. Zheludev, "Planar metamaterial with transmission and reflection that depend on the direction of incidence," Appl. Phys. Lett. **94**(13), 131901 (2009).
15. S. V. Zhukovsky, A. V. Novitsky, and V. M. Galynsky, "Elliptical dichroism: operating principle of planar chiral metamaterials," Opt. Lett. **34**(13), 1988–1990 (2009).
16. S. V. Zhukovsky, C. Kremers, and D. N. Chigrin, "Plasmonic rod dimers as elementary planar chiral meta-atoms," Opt. Lett. **36**(12), 2278–2280 (2011).
17. A. V. Novitsky, V. M. Galynsky, and S. V. Zhukovsky, "Asymmetric transmission in planar chiral split-ring metamaterials: microscopic Lorentz-theory approach," Phys. Rev. B **86**(7), 075138 (2012).

#174160 - $15.00 USD Received 10 Aug 2012; revised 19 Sep 2012; accepted 20 Sep 2012; published 1 Nov 2012

18. R. Singh, E. Plum, C. Menzel, C. Rockstuhl, A. K. Azad, R. A. Cheville, F. Lederer, W. Zhang, and N. I. Zheludev, "Terahertz metamaterial with asymmetric transmission," Phys. Rev. B **80**(15), 153104 (2009).
19. R. Singh, I. A. I. Al-Naib, M. Koch, and W. Zhang, "Asymmetric planar terahertz metamaterials," Opt. Express **18**(12), 13044–13050 (2010).
20. B. Bai, Y. Svirko, J. Turunen, and T. Vallius, "Optical activity in planar chiral metamaterials: Theoretical study," Phys. Rev. A **76**(2), 023811 (2007).
21. D. H. Kwon, P. L. Werner, and D. H. Werner, "Optical planar chiral metamaterial designs for strong circular dichroism and polarization rotation," Opt. Express **16**(16), 11802–11807 (2008).
22. M. Decker, M. W. Klein, M. Wegener, and S. Linden, "Circular dichroism of planar chiral magnetic metamaterials," Opt. Lett. **32**(7), 856–858 (2007).
23. M. Tonouchi, "Cutting-edge terahertz technology," Nat. Photonics **1**(2), 97–105 (2007).
24. B. Ferguson and X. C. Zhang, "Materials for terahertz science and technology," Nat. Mater. **1**(1), 26–33 (2002).
25. S. Zhang, Y.-S. Park, J. Li, X. Lu, W. Zhang, and X. Zhang, "Negative refractive index in chiral metamaterials," Phys. Rev. Lett. **102**(2), 023901 (2009).
26. W.-H. Sun, Y.-J. Bao, M. Wang, and R.-W. Peng, "C. Sun X. Lu, J. Shao, Z-F. Li, and N-B. Ming, "Construction of a chiral metamaterial with a U-shaped resonator assembly," Phys. Rev. B **81**, 075119 (2010).
27. J. Zhou, J. Dong, B. Wang, Th. Koschny, M. Kafesaki, and C. M. Soukoulis, "Negative refractive index due to chirality," Phys. Rev. B **79**(12), 121104(R) (2009).
28. B. Wang, J. Zhou, T. Koschny, and C. M. Soukoulis, "Nonplanar chiral metamaterials with negative index," Appl. Phys. Lett. **94**(15), 151112 (2009).
29. B. Wang, J. Zhou, Th. Koschny, M. Kafesaki, and C. M. Soukoulis, "Chiral metamaterials: simulations and experiments," J. Opt. A, Pure Appl. Opt. **11**(11), 114003 (2009).
30. A. V. Rogacheva, V. A. Fedotov, A. S. Schwanecke, and N. I. Zheludev, "Giant gyrotropy due to electromagnetic-field coupling in a bilayered chiral structure," Phys. Rev. Lett. **97**(17), 177401 (2006).
31. M. Decker, M. Ruther, C. E. Kriegler, J. Zhou, C. M. Soukoulis, S. Linden, and M. Wegener, "Strong optical activity from twisted-cross photonic metamaterials," Opt. Lett. **34**(16), 2501–2503 (2009).
32. A. Andryieuski, C. Menzel, C. Rockstuhl, R. Malureanu, F. Lederer, and A. Lavrinenko, "Homogenization of resonant chiral metamaterials," Phys. Rev. B **82**(23), 235107 (2010).
33. N. Liu and H. Giessen, "Three-dimensional optical metamaterials as model systems for longitudinal and transverse magnetic coupling," Opt. Express **16**(26), 21233–21238 (2008).
34. R. Zhao, Th. Koschny, E. N. Economou, and C. M. Soukoulis, "Comparison of chiral metamaterial designs for repulsive Casimir force," Phys. Rev. B **81**(23), 235126 (2010).
35. Z. Li, R. Zhao, Th. Koschny, M. Kafesaki, K. B. Alici, E. Colak, H. Caglayan, E. Ozbay, and C. M. Soukoulis, "Chiral metamaterials with negative refractive index based on four 'U' split ring resonators," Appl. Phys. Lett. **97**(8), 081901 (2010).
36. M. Decker, R. Zhao, C. M. Soukoulis, S. Linden, and M. Wegener, "Twisted split-ring-resonator photonic metamaterial with huge optical activity," Opt. Lett. **35**(10), 1593–1595 (2010).
37. R. Zhao, L. Zhang, J. Zhou, Th. Koschny, and C. M. Soukoulis, "Conjugated gammadion chiral metamaterial with uniaxial optical activity and negative refractive index," Phys. Rev. B **83**(3), 035105 (2011).
38. C. Menzel, C. Rockstuhl, and F. Lederer, "Advanced Jones calculus for the classification of periodic metamaterials," Phys. Rev. A **82**(5), 053811 (2010).
39. M. Kafesaki, I. Tsiapa, N. Katsarakis, Th. Koschny, C. M. Soukoulis, and E. N. Economou, "Left-handed metamaterials: the fishnet structure and its variations," Phys. Rev. B **75**(23), 235114 (2007).
40. J. D. Jackson, *Classical Electrodynamics*, 3rd ed. (Wiley, New York, 1998).
41. J. A. Kong, *Electromagnetic Wave Theory* (EMW Publishing, Cambridge, MA, 2008).
42. R. Zhao, Th. Koschny, and C. M. Soukoulis, "Chiral metamaterials: retrieval of the effective parameters with and without substrate," Opt. Express **18**(14), 14553–14567 (2010).
43. S. Zhang, J. Zhou, Y. S. Park, J. Rho, R. Singh, S. Nam, A. K. Azad, H. T. Chen, X. Yin, A. J. Taylor, and X. Zhang, "Photoinduced handedness switching in terahertz chiral metamolecules," Nat Commun **3**, 942 (2012).

## 1. Introduction

Metamaterials are tailored man-made composite materials, made of sub-wavelength building structures, possessing different properties from those of their constituent materials. These properties mainly result from the geometry of the building structures. Designing properly these structures one can achieve unique metamaterial properties, beyond those of natural materials, such as negative magnetic permeability, negative refractive index, and extreme permittivity or permeability values (i.e. close to zero or very large values) [1–3]. These novel properties can lead to new possibilities and solutions in a variety of potential applications, from telecommunication and information processing, to imaging, security and sensing. In particular, negative refractive index metamaterials can provide in principle perfect lensing (i.e. with a resolution beyond the diffraction limit), leading to new possibilities in imaging, lithography and data storage devices; moreover, they exhibit backwards propagation (i.e. opposite phase and energy velocity), which can be exploited in a variety of

#174160 - $15.00 USD Received 10 Aug 2012; revised 19 Sep 2012; accepted 20 Sep 2012; published 1 Nov 2012

telecommunication devices, like antennas, filters, waveguides, transmission lines and so on [2–5].

A very interesting and particularly useful category of metamaterials is the chiral metamaterials, as they offer great possibilities in the control of the light polarization [6,7]. In chiral metamaterials, optical activity (i.e. polarization rotation of a linearly polarized wave) and circular dichroism (i.e. the absorption difference between left- and right-handed circularly polarized light) can exceed the corresponding effects in natural chiral materials by many orders of magnitude. Hence, chiral electromagnetic metamaterials are interesting candidates for future polarization control applications such as designer wave-plates and polarization filters [8]. The huge chirality in chiral metamaterials was also recently proposed to reduce the attractive Casimir force which is detrimental in micro- and nano- electromechanical systems [9,10].

Another interesting capability of chiral metamaterials is that they can provide negative refractive index for circularly polarized light [11,12]. This chirality approach for the achievement of negative index is an alternative to the more common approach which requires combination of negative permeability and negative permittivity.

Besides the regular three-dimensional (3D) chiral metamaterials that lack any mirror symmetry plane, recently, planar chiral metamaterials (PCM) have been also introduced [13–22]. These are planar structures (thus the plane of the structure is a mirror symmetry plane) where the "meta-atoms" cannot be superimposed with their in-plane mirror image without being lift-off the plane (they present 2D rather than 3D enantiomeric asymmetry). This form of PCM leads to asymmetry in the propagation of electromagnetic waves incident from opposite directions, resulting to asymmetric transmission and other novel and unique propagation characteristics, in principle different than those of regular 3D chiral metamaterials.

The majority of today's metamaterials, especially negative index metamaterials (NIMs), operate in the microwave part of the electromagnetic spectrum, while there is a great interest and effort to extend their operation regime to higher frequencies, from THz to the optical regime. The extension of metamaterial operation in the THz regime and the realization of metamaterial-based THz components is a task of particular technological importance. This is due to the fact that the majority of natural materials do not show strong response in the THz regime; thus they are not offered for the realization of THz manipulation, although the technological importance of the THz radiation, especially in domains like imaging and security [23,24] is well recognized. To that extent, chiral metamaterials operating in the THz regime, due to their great potential for polarization control, can provide a valuable tool for the polarization manipulation of THz waves. However, very few attempts to realize and demonstrate THz chiral metamaterials have been made up to now [25,26]. Most of the existing chiral metamaterial structures concern microwave metamaterials, while there are also already a few studies on optical chiral structures. Concerning chiral microwave metamaterials, the existing studies have provided a variety of chiral designs that are very easy to fabricate and show giant optical activity and circular dichroism, as well as negative index of refraction [27–30]. The existing optical chiral structures are in their majority miniaturized replicas of the microwave structures [31,32].

In this work we demonstrate both theoretically and experimentally extremely large optical activity (~420°/wavelength), large circular dichroism and negative refractive index in five different chiral metamaterial structures/designs operating in the THz regime. The designed structures are made of paired conductors; they have been fabricated using UV lithography, alternating metal and polyimide, and they are fully flexible. Two of our designs have been already proposed and studied in the microwaves and in the optical regime, showing quite interesting polarization control capabilities. The rest three designs are proposed here for the first time, showing dual band pure optical activity and negative refractive index for both left-handed and right-handed circularly polarized waves.

#174160 - $15.00 USD Received 10 Aug 2012; revised 19 Sep 2012; accepted 20 Sep 2012; published 1 Nov 2012

## 2. The designs

The chiral structures employed in the present study are introduced in Fig. 1, while their geometrical features are presented in Table 1. The first design [Fig. 1(a)] is an assembly of double-layered metallic U-shaped resonators (U-SRRs), where each U-SRR of the upper layer is rotated by 90° in respect to its counterpart of the lower layer. The in-plane unit-cell contains four U-SRRs mutually rotated as to ensure fourfold rotational symmetry of the system. This three dimensional structure was first numerically mentioned in [33] and then firstly proposed for the construction of chiral metamaterials numerically in [34], and subsequently experimentally studied in GHz [35], THz [26], and optical frequency range [36]. It was found that a pure optical activity (i.e. polarization rotation with no ellipticity) as high as 807° per wavelength and 417° per wavelength can occur in the GHz and optical regime, respectively, associated with sufficiently high (more than 40%) transmission. The next two designs are new designs, based on the conjugated gammadion structure [37]. They consist of a pair of crosses with Z-type arms, as shown in Fig. 1(b) and Fig. 1(c). The unit cell of the fourth chiral design of Fig. 1 [see Fig. 1(d)] is composed of a pair of silver crosses *(cross-wires design)* rotated against each other by an angle of $\varphi = 30°$. A similar design was first studied in GHz range [27], where it showed a pure optical activity as high as 448° per wavelength (at 7 GHz) and negative index of refraction, and subsequently in the optical regime [31], showing optical activity 62° per wavelength (at 220 THz) but no negative index. The last chiral design of Fig. 1 [see Fig. 1(e)] is also a design proposed here for the first time. Its unit cell consists of a pair of silver squares *(square-pairs design)* rotated against each other by an angle $\varphi = 25°$. In all designs the conjugated arrangement of the metallic resonators is such as to lead to no center of inversion and no mirror-symmetry plane for the structure, which, in combination with the C4 rotational symmetry of all the designs [37,38], ensures pure chiral response, i.e. that the eigenmodes in all cases are the pure circularly polarized waves.

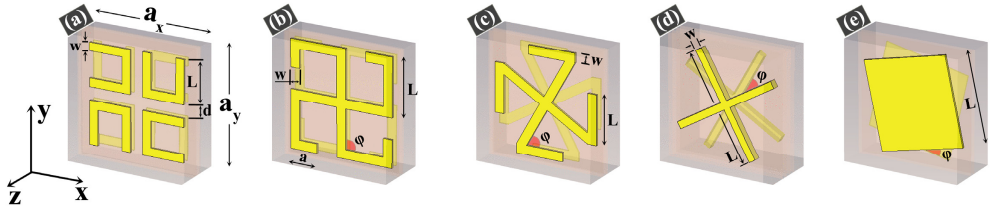


Fig. 1. Schematic of the unit cell of the chiral metamaterials under consideration: (a) two relatively rotated layers of four U-SRRs, (b) and (c) two relatively rotated layers of Z-type crosses with φ = 90° and φ = 60°, respectively, (d) two relatively rotated layers of cross-wires and (e) design based on two relatively rotated squares. The metal (yellow-color) thickness $t_m$ and the dimensions $a_x$, $a_y$, $L$, $w$, $a$, $d$ and $\varphi$, for each design are presented in Table 1. The wave propagation is along the $z$ direction.

**Table 1. Dimensions (in microns) of chiral metamaterials under consideration (see Fig. 1)**

| Chiral metamaterial | $a_x$ | $a_y$ | $t_m$ | L | w | d | a | φ |
|---|---|---|---|---|---|---|---|---|
| U-SRRs, Fig. 1(a) | 29.0 | 29.0 | 0.5 | 10.0 | 2.0 | 3.0 | - | - |
| Z-type crosses with φ = 90°, Fig. 1(b) | 26.0 | 26.0 | 0.5 | 12.5 | 2.0 | - | 4.0 | 90 |
| Z-type crosses with φ = 60°, Fig. 1(c) | 26.0 | 26.0 | 0.5 | 10.5 | 2.0 | - | - | 60 |
| Cross-wires, Fig. 1(d) | 17.0 | 17.0 | 1.0 | 16.0 | 1.0 | - | - | 30 |
| Square-pairs, Fig. 1(e) | 20.5 | 20.5 | 0.4 | 15.0 | - | - | - | 25 |

#174160 - $15.00 USD Received 10 Aug 2012; revised 19 Sep 2012; accepted 20 Sep 2012; published 1 Nov 2012

## 3. Fabrication and characterization approaches

The fabrication of our chiral structures has been done using UV-lithography, in an alternating layer-by-layer fashion of polyimide and silver. We used a standard spin-on polyimide (DuPont Pyralin SP series PI-2525) with a dielectric constant of 2.9. The sequence of layers starts by spinning and curing a 5 μm thick layer of polyimide on a Si substrate. A silver film (with a thickness $t_m$ of 0.5 or 1.0 μm, depending on the design) is deposited on top and patterned by use of standard lift-off techniques. Another layer of polyimide (spacer layer) is spun on over the metallic layer and cured. The thickness of this polyimide layer is 1 μm. Another metal layer is deposited and patterned (see Fig. 1 for details), while the sequencing of layers continues with another 5 μm thick polyimide layer. The layer-to-layer alignment was done with a Karl Suss MA6 mask aligner and UV photolithography. The alignment accuracy is of the order of 0.5 μm. After the fabrication, the polyimide-encapsulated metallic chiral structures were removed from the Si substrate. The resultant samples are polymer based and flexible, with an area of 15 mm × 15 mm and thickness between 11.8 μm and 13 μm (depending on the design).

The characterization of the samples was performed in the frequency regime 2-12 THz, which is below the polyimide absorption bands (~12 THz and ~20 THz). The experimental characterization was done through transmission measurements, which were performed using a Bruker IFS 66v/S Fourier-transform infrared spectrometer (with a collimated beam) and two linear polyethylene grid polarizers.

The results of the measurements were compared in all cases with corresponding transmission simulations. For the simulations we used a commercial three-dimensional full-wave solver (CST Microwave Studio, Computer Simulation Technology GmbH, Darmstadt, Germany) based on the Finite Integration Technique. For each chiral design we considered in the simulations a single unit cell, as shown in Fig. 1, with periodic boundary conditions along $x$ and $y$ directions, while an incident plane wave propagating along $z$-direction was used to excite the structure.

## 4. Results and discussion

Since the experimental data taken from the Bruker IFS 66v/S FT-IR spectrometer are obtained by linearly polarized fields, four transmission components, $T_{xx}$, $T_{xy}$, $T_{yx}$ and $T_{yy}$, can be measured, where the first and second lower indices indicate the output and input signal polarizations, respectively, e.g. $T_{xy} = E_x^t / E_y^i$, where $E_y^i$ is the input $y$-polarized electric field and $E_x^t$ is the transmitted $x$-polarized electric field [28]. Due to the four-fold rotational symmetry of our structures $T_{xx} = T_{yy}$ and $T_{xy} = -T_{yx}$, so only two transmission amplitudes, e.g., $T_{xx}$ and $T_{xy}$, are needed to be considered. Indeed, examining all four transmission components in both the experimental and the simulation data we found that the quantities $T_{xx}$-$T_{yy}$ and $T_{xy}$ + $T_{yx}$ (not shown here) do not exceed $3.5 \times 10^{-3}$; thus only $T_{xx}$ and $T_{xy}$, are taken into account in the discussion below.

#174160 - $15.00 USD Received 10 Aug 2012; revised 19 Sep 2012; accepted 20 Sep 2012; published 1 Nov 2012

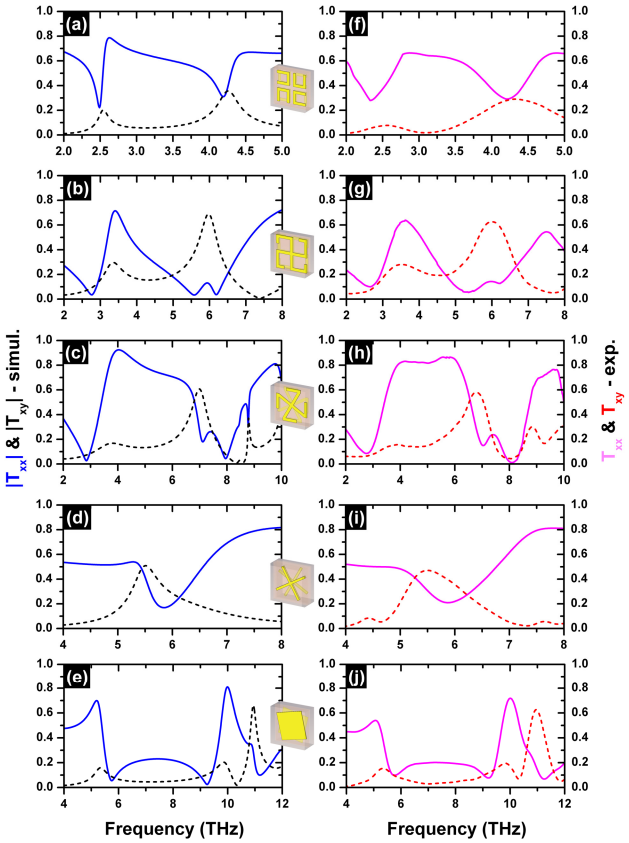


Fig. 2. Simulated (left column) and measured (right column) magnitude of the transmission components ($T_{xx}$: solid lines, $T_{xy}$: dashed lines), for the chiral metamaterials under consideration and for linearly polarized incident wave. The insets show the correspond designs.

In Fig. 2 we show both the experimental (right column) and simulated (left-column) transmission amplitudes $|T_{xx}|$ and $|T_{xy}|$ for all the designs studied. Besides the very good quantitative agreement between simulations and experiments, one can observe in Fig. 2 a slight broadening of the resonance dips in the experimental cases (compared to the theory) due to the non-uniformity in the fabrication of the samples. (Since the simulated transmission results of Fig. 2 are in very good agreement with the corresponding measurement results, we restrict the subsequent calculations and analysis to the simulation results only, where phase information is also available.)

As can be observed in Figs. 2(a) and 2(f), the U-SRR structure shows two distinct resonances. This is in agreement with the discussion of [35], where the resonances and the associated current modes are described in detail.

Observing the response of the structures of Figs. 2(b) and 2(g) as well as Figs. 2(c) and 2(h), one can see a more complicated spectrum with more resonances in $T_{xx}$ and larger cross-polarized transmission levels, indicating larger optical activity. This response will be analyzed in more detail later on.

The structure of Figs. 2(d) and 2(i), as was mentioned also in the previous section, has been studied both in GHz and the optical regime. There, it showed two distinct low-frequency resonances which were classified as “magnetic” (the lower one - associated with antiparallel currents in the equivalent branches of the pair) and “electric” (the higher one - associated with parallel currents in the equivalent branches of the pair). The absence of these two distinct

#174160 - $15.00 USD Received 10 Aug 2012; revised 19 Sep 2012; accepted 20 Sep 2012; published 1 Nov 2012

resonances in our case is due to the fact that these two resonances in our particular geometry lie very close to each other, being thus indistinguishable in the transmission picture.

As discussed in [39], in a wire-pair system a way to move the electric dipole-like resonance well above the magnetic one is to make the wires wider, taking the form of slabs. This is verified in the case of Figs. 2(e) and 2(j), where the wires of Figs. 2(d) and 2(i) have been replaced by square slabs and the double-resonance picture has been established.

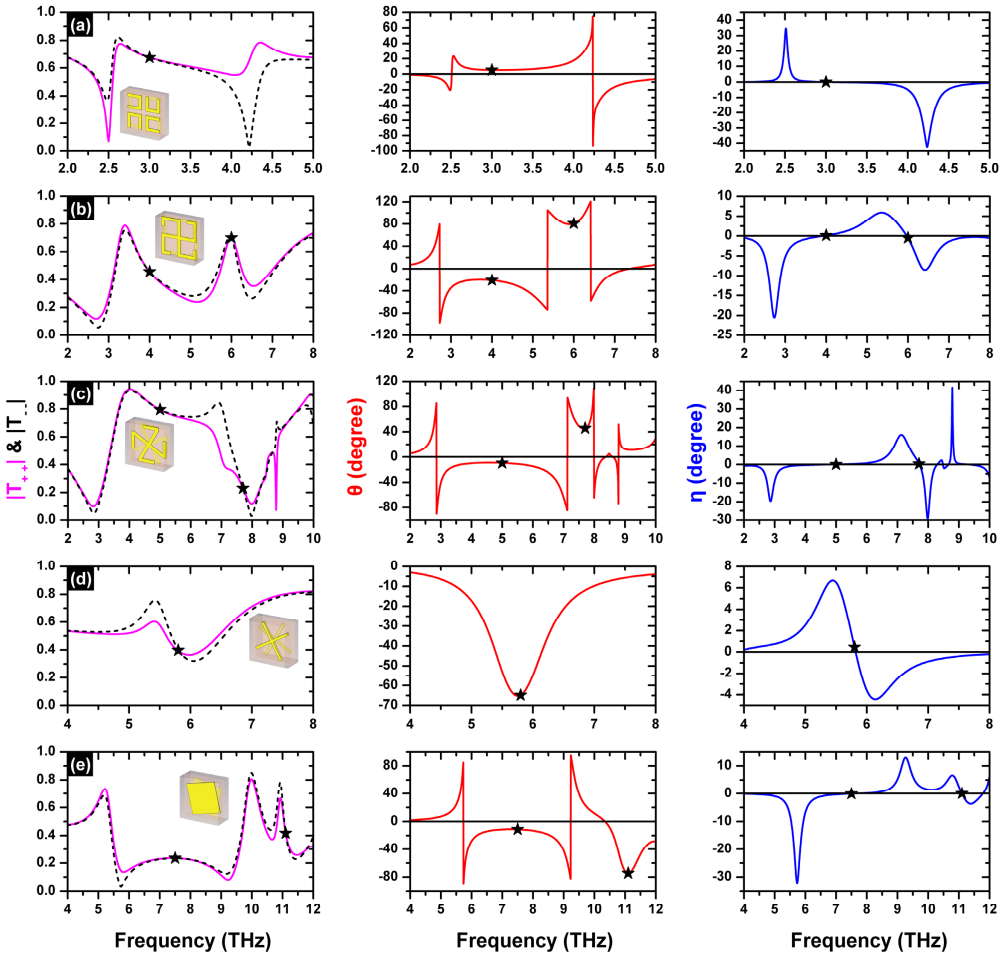


Fig. 3. *Left column:* Simulated magnitude of the transmission coefficients for the right circularly polarized, $|T_{++}|$ (solid lines), and the left circularly polarized, $|T_{-+}|$ (dashed lines), electromagnetic wave, for all the designs studied here. The *middle column* shows the simulated azimuth rotation angle, $\theta$, for each of the designs and the *right column* the corresponding simulated ellipticity, $\eta$. The insets show the corresponding design, while black stars indicate the points where $\eta \approx 0$.

One worth-noticing feature of Fig. 2 is the regimes of large cross-polarized transmission ($T_{xy}$) in all the structures studied, indication of large optical activity. To obtain a full picture of the optical activity of our structures and of their capabilities to create polarization manipulation components, one needs to study and analyze the transmission results for circularly polarized waves. These results can be directly calculated from the linearly polarized transmission data [27] according to the equation

#174160 - $15.00 USD Received 10 Aug 2012; revised 19 Sep 2012; accepted 20 Sep 2012; published 1 Nov 2012

$$\begin{pmatrix} T_{++} & T_{+-} \\ T_{-+} & T_{--} \end{pmatrix} = \frac{1}{2} \times \begin{pmatrix} \left(T_{xx} + T_{yy}\right) + i\left(T_{xy} - T_{yx}\right) & \left(T_{xx} - T_{yy}\right) - i\left(T_{xy} + T_{yx}\right) \\ \left(T_{xx} - T_{yy}\right) + i\left(T_{xy} + T_{yx}\right) & \left(T_{xx} + T_{yy}\right) - i\left(T_{xy} - T_{yx}\right) \end{pmatrix}, \qquad (1)$$

which in our case can be simplified to $T_{++} = T_{xx} + iT_{xy}$, $T_{--} = T_{xx}$-$iT_{xy}$, $T_{+-} = T_{-+} = 0$. In the above relations the subscript + denotes the right-handed circularly polarized wave (RCP, + ) and the subscript − the left-handed circularly polarized wave (LCP, −), while the first subscript again denotes the polarization of the transmitted wave and the second the polarization of the incident wave.

The transmission amplitudes for circularly polarized waves, $T_{++}$ and $T_{--}$ [obtained through Eq. (1)], for all our chiral structures are shown in the left column of Fig. 3. The cross polarized transmissions $T_{-+}$ and $T_{+-}$ (not shown here) are below $1.8 \times 10^{-2}$ (less than −35dB at the resonance frequencies for all the structures), and thus can be considered as negligible, which further verifies that all our chiral metamaterial designs are pure chiral structures where the eigenwaves are the circularly polarized modes.

If we focus on the U-SRR structure [Fig. 3(a)], one can notice that the transmission response is different for RCP and LCP waves, especially at the two resonance frequencies of the structure, at $f$ = 2.5 THz and 4.2 THz, showing a strong circular dichroism (defined as $|T_{++}|^2 - |T_{--}|^2$). In fact the U-SRR structure shows the stronger and most broad-band circular dichroism among all the designs studied here. Considerable dichroism is shown also in the Z-shaped structure of Fig. 3(c), around 7 THz.

To fully characterize the dichroic response and the polarization control capabilities of our structures, we further analyze the transmission results, calculating the polarization azimuth rotation angle and the ellipticity of the transmitted wave. The polarization azimuth rotation angle $\theta$ (for a linearly polarized incident wave this is the angle between the major ellipse axis of the elliptically polarized transmitted wave with the polarization of the incident wave), indicative of the optical activity of the structures, can be calculated as $\theta = [\arg(T_{++}) - \arg(T_{--})]/2$ [29,36,40], while the ellipticity of the transmitted wave is defined as $\eta = \frac{1}{2}\sin^{-1}\left(\frac{|T_{++}|^2 - |T_{--}|^2}{|T_{++}|^2 + |T_{--}|^2}\right)$ [29,36,40] (zero $\eta$ corresponds to linearly polarized transmitted wave, while 45° corresponds to right-handed circularly polarized wave (RCP) and −45° corresponds to left-handed circularly polarized wave (LCP); intermediate values indicate elliptically polarized wave).

The simulated azimuth rotation angle, $\theta$, and the ellipticity, $\eta$, for each of our chiral metamaterials are shown in the second and third columns of Fig. 3, respectively, next to the corresponding transmission data. As one can see from Fig. 3, frequency regimes of pure optical activity (optical activity with $\eta \approx 0$) exist in all our structures; this optical activity in some case is extremely large and/or quite broad-band. The pure optical activity values for each structure are listed in Table 2.

If we focus on the U-SRR design [Fig. 3(a)], one can notice that the frequency regime of nearly pure optical activity, which lies between the two resonance frequencies of the structure, is very broad (of width ~1 THz). The optical activity achieved there is 43 degrees/wavelength. Another worth-mentioning feature of the structure is the large ellipticity (~42.5°) at ~4.2 THz, indicating an almost circularly polarized transmitted wave and thus the capability of the structure to work as a circular polarization filter and circular polarizer.

#174160 - $15.00 USD Received 10 Aug 2012; revised 19 Sep 2012; accepted 20 Sep 2012; published 1 Nov 2012

**Table 2. Pure optical activity (optical activity with η≈0) in some frequency range for each of the chiral structures under consideration, as shown in Fig. 3**

| Structure | Spectral range with $\eta \approx 0$ (% of total range) | Transmission level | Optical activity (degrees/wavelength) at $\eta \approx 0$ |
|---|---|---|---|
| U-SRRs, Fig. 1(a) | 2.6-3.8 THz (40%) | 68% | 43° at 3.0 THz |
| Z-type crosses with φ = 90°, Fig. 1(b) | 3.5-4.5 THz (25%) | 46% | 132° at 4.0 THz |
| | 5.5-6.2 THz (11.7%) | 70% | 338° at 6.0 THz |
| Z-type crosses with φ = 60°, Fig. 1(c) | 3.5-6.0 THz (50%) | 80% | 48° at 5.0 THz |
| | 7.5-7.9 THz (5.2%) | 23% | 149° at 7.7 THz |
| Cross-wires, Fig. 1(d) | 5.6-6.2 THz (10.1%) | 40% | 257° at 5.8 THz |
| Square-pairs, Fig. 1(e) | 6.5-8.2 THz (22.7%) | 24% | 38° at 7.5 THz |
| | 11.0-11.4 THz (3.5%) | 42% | 171° at 11.1 THz |

In the next two designs [see Figs. 3(b) and 3(c)] one can see two frequency regimes of quite large pure optical activity in each structure, with the higher frequency regime to show giant activity, larger than 300 degrees/wavelength (see Table 2). The finding above means that for a linear polarization incident wave, the transmission wave is still linear polarized but rotates by an angle $\theta$~81° at ~6 THz, which is ~338° per wavelength.

Focusing on the cross-wire structure of Fig. 3(d), we also see a quite large optical activity, significantly higher than in the optical analog of the structure (where it is 62° per wavelength). This optical activity could become even higher (reaching 1100° per wavelength) and more broadband without the presence of the thick outermost polyimide top and bottom layer encapsulating the structure, as related calculations reveal (not shown here).

Finally, in the slab-pair structure of Fig. 3(f), one can observe a very high ellipticity of the transmitted wave at the lower-frequency resonance of the structure; this ellipticity can reach 45° without the presence of the top and bottom polyimide layers, indicating the circular polarization filtering and circular polarizer capabilities of the design.

In the last part of this section we examine the potential of our structures to give backward propagation and negative refractive index response. This is done by calculating the effective refractive index for LCP and RCP polarized light, $n_-$ (or $n_{\mathrm{LCP}}$) and $n_+$ (or $n_{\mathrm{RCP}}$) respectively. The refractive indices are given by $n_\pm = n \pm \kappa$, where $\eta = \sqrt{\varepsilon\mu}$, with $\varepsilon$ and $\mu$ the relative effective permittivity and permeability of the structure, respectively, and $\kappa$ the chirality parameter, as defined, e.g., in [41]. The effective indices calculation here is done by applying the retrieval procedure for chiral metamaterials which is reported in [42].

Figure 4 shows the retrieved effective parameters $n_\pm$, $n$, $\kappa$, based on the simulation data of the transmission and reflection for all our chiral structures. We can see that all the structures exhibit frequency regimes (around the resonances of the chirality parameter $\kappa$) where refractive index is negative either for LCP or for RCP light.

#174160 - $15.00 USD Received 10 Aug 2012; revised 19 Sep 2012; accepted 20 Sep 2012; published 1 Nov 2012

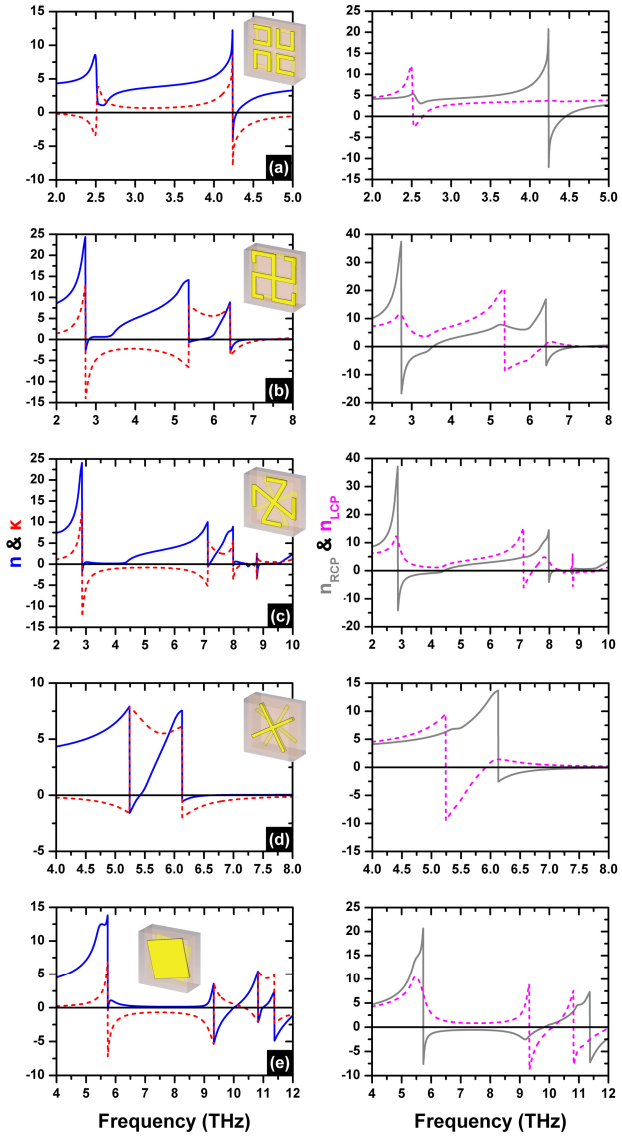


Fig. 4. Retrieved effective parameters of the chiral metamaterials under consideration. *Left column:* Real parts of the refractive index $n$ (solid blue lines) and the chirality $\kappa$ (dashed red lines). The insets show the corresponding design. *Right column:* Real parts of the refractive indices for RCP (solid grey lines) and LCP waves (dashed magenta lines).

## 5. Conclusions

We have studied, both theoretically and experimentally, the wave propagation characteristics in five different chiral metamaterial structures in the THz regime. The structures are embedded in a polyimide layer, and they are fully flexible. The study has been done through transmission simulations and measurements for linearly polarized waves, where the circularly polarized transmission, the optical activity and the ellipticity of the transmitted wave have been calculated from. We found in almost all our structures larger optical activity in more than a single frequency regime. Moreover using a retrieval procedure to calculate the effective parameters, we showed in all our structures negative refractive index response for both left-handed and right-handed circularly polarized light. The large optical activity and circular

#174160 - $15.00 USD Received 10 Aug 2012; revised 19 Sep 2012; accepted 20 Sep 2012; published 1 Nov 2012

dichroism response make our proposed designs valuable candidates for development of THz manipulation components like circular polarization filters, polarizers, wave-plates, etc. The flexibility of our samples opens the opportunity to realize tunable chiral metamaterials [7,43] using external mechanical forces, which will result in plenty of applications.

**Acknowledgments**

Authors would like to acknowledge the support by EU, through projects NIMNIL, by-NANOERA and the COST action MP0803. Work at Ames Laboratory was partially supported by the Department of Energy (Basic Energy Sciences) under Contract No. DE-AC02-07CH11358 (computational studies). Fruitful discussions with Dr. Thomas Koschny are also acknowledged.

#174160 - $15.00 USD Received 10 Aug 2012; revised 19 Sep 2012; accepted 20 Sep 2012; published 1 Nov 2012